Bistatic RCS Measurements of Large Targets in a Compact Range

Monique Potgieter, Johann W. Odendaal, *Senior Member, IEEE*, Ciara Blaauw and Johan Joubert, *Senior Member, IEEE*

***Abstract*— This paper illustrates the ability to perform bistatic radar cross section (RCS) measurements at a fixed bistatic angle in a compact range. Literature regarding bistatic RCS measurements in compact ranges is limited. The traditional setup of a compact range was adapted to perform bistatic RCS measurements. These bistatic measurements were conducted on canonical and complex realistic scale airframe models. The targets were illuminated with a plane wave created by an offset parabolic dish reflector. The bistatic scattering of the targets were measured by placing a receive antenna at a fixed bistatic angle and finite distance in the compact range. This paper also investigates the effect of the finite separation between the targets and the receiver on the bistatic scattering measurements of large complex targets. The accuracy of the bistatic RCS measurements are compared to full-wave simulations conducted with FEKO using the Multi-Level Fast Multipole Method (MLFMM) solver. Quantitative comparisons are drawn between the simulations and measurements using the Feature Selective Validation (FSV) method.**

***Index Terms*— Bistatic radar, compact range, measurements, radar cross section**

I. Introduction

Indoor radar cross section (RCS) measurements are usually conducted in a controlled environment, e.g. an anechoic chamber or compact range. A compact range is specifically well suited for monostatic RCS measurements. Bistatic RCS measurements, from literature, are predominantly conducted in anechoic chambers, as these chambers are more readily available and allows bistatic RCS measurements at different bistatic angles by sweeping the receive antenna around the target at a constant radius. The finite separations between the transmit/receive antennas and the target limit the size of targets that can be measured complying with the far field criteria. A compact range illuminates a target with a plane wave and allows for far-field measurements to be conducted in a small area [1], [2]. Literature concerning bistatic RCS measurements of targets in a compact range is limited and restricted to measurements at fixed bistatic angles.

In 1993 one study investigated the ability to perform bistatic RCS measurements in a compact range by measuring the bistatic scattering of an electrically large PEC flat plate [1]. This measurement setup consisted of a transmit antenna and a receive antenna which were positioned on either side of the focal point, defocusing the parabolic reflector. Bistatic measurements were performed at two fixed bistatic angles viz., $\beta = 15°$ and $\beta = 24°$. The accuracy of the measured data was investigated by comparing the results to physical optics simulations. Some misalignment issues were observed and it was concluded that bistatic RCS measurements can be performed in the compact range provided that a small target is measured at small bistatic angles. The bistatic scattering of a complex scale model FLAMME stealth model was measured at the BABI bistatic anechoic measurement facility [3]. The bistatic facility is an anechoic chamber capable of transmitting and receiving co- and cross-polarized CW signals from 1 GHz to 18 GHz. The measurement setup consists of a transmitter and receiver that are swept at a constant radius around the target. The far-field criteria limited the measurements of the complex stealth target to 4 GHz. At this frequency the target had an electrical size of approximately 8λ.

In 2004 a study by Daout et. al. investigated the ability to perform bistatic RCS measurements in the Boris Vian anechoic chamber [4]. This chamber was originally designed for antenna measurements over a frequency range from 2 GHz to 18 GHz. A small PEC circular cylinder was used as a target to test the anechoic chamber. The target to antennas distance remained constant during the measurements. The receiver was swept on a circular path around the target. With this setup a forward RCS scattering of greater than -13 dBsm could be measured with a ± 0.9 dB uncertainty.

A study in 2006 investigated the ability to perform bistatic RCS measurements in a compact range using cylindrical near-field measurements [5]. The target was illuminated with the compact range reflector and the bistatic scattering from the target was measured with a cylindrical near-field scanner. The far-field scattering was computed from near-field measurements and compared to numerical calculations. This study only investigated the ability to measure the bistatic scattering of two canonical targets viz., a sphere and a cylinder. Accurate agreement between the bistatic RCS calculated from near-field measurements and the numerical RCS were obtained over a bistatic angular range from 60° to 300°. Large differences were noted at other bistatic angular ranges. Drawbacks of this measurement configuration are stability and the precise mechanical positioning which is required.

The ability to perform bistatic RCS measurements, on canonical and complex realistic airframe targets at fixed bistatic angles, in the compact range at the University of Pretoria is illustrated in this study. The accuracy of the measurements is investigated by comparing the measured data to simulations performed in FEKO using MLFMM [6]. The measured and simulated results are analyzed using the Feature Selective Validation (FSV) method [7]. The FSV method assesses the correlation between two datasets and provides a quantitative comparison between the measured and simulate bistatic RCS results.

II. Measurement Setup

The study by Bradley et. al. [8] lists a few capabilities which a measurement facility should have in order to perform reliable bistatic RCS measurements. These capabilities include (i) the ability to precisely align the target; (ii) the ability to repeat measurements and obtain the same results; (iii) good transmit and receive antenna polarization; (iv) low background noise; (v) the ability to perform fixed or swept bistatic angle measurements; and (vi) ease of measurement setup. Very accurate measurements can be performed in a compact range but according to [9] there are several sources that can cause measurement inaccuracy in these measurement facilities. These include (i) antenna coupling; (ii) reflections; (iii) system distortion; (iv) target alignment error; and (v) near-field effects.

Manuscript received May, 2018. This work is based on the research supported by the National Research Foundation (NRF) of South Africa (Grand Number 114941) and the Council for Scientific and Industrial Research (CSIR).

M. Potgieter and C. Blaauw are with the Centre of Electromagnetism, University of Pretoria and with the CSIR Defence, Peace, Safety and Security, Pretoria 0002, South Africa (email: u11175100@tuks.co.za).

J.W. Odendaal and J. Joubert are with the Centre of Electromagnetism, University of Pretoria, Pretoria 0002, South Africa.

Inaccuracies caused by antenna coupling become more apparent at large bistatic angles if the receive antenna is in the main beam of the transmitter. The reflections off chamber walls are decreased by covering the inside of the compact range with absorbing material. The edges of the reflector are usually serrated or rolled to reduce the edge diffraction field contribution in the quiet zone [10]. System distortion refers to cross-polarization impurities. Near-field effects are observed when the target is physically too big and is not completely illuminated by the plane wave. The target is thus illuminated with different phase centers over its surface, which results in a difference in the scattering of the target. The compact range at the University of Pretoria, South Africa, is traditionally used for antenna characterization and monostatic RCS measurements. The compact range was reconfigured to perform bistatic RCS measurements. The compact range met all the criteria listed by Bradley et. al. to perform accurate bistatic measurements, except only fixed bistatic angle measurements could be conducted.

The bistatic RCS measurements in the reconfigured compact range were performed by illuminating the target with a plane wave created by an offset parabolic dish reflector. A receive antenna was mounted to the side of the chamber at a finite distance and fixed bistatic angle. In a previous study, bistatic measurements were conducted on canonical targets at larger fixed bistatic angles viz. $\beta = 45°$ and $\beta = 90°$, [11] and the ability to perform full-polarimetric bistatic RCS measurements in the compact range was investigated [12]. In this paper, measurements conducted on complex PEC targets at $\beta = 30.8°$ are presented for VV-polarization. A bistatic angle of 30.8° was used as it resulted in the furthest distance from the target to the receiver in the compact range.

A photo of the bistatic measurement setup of a canonical missile and a 1:25 Boeing 707 scale model are provided in Fig. 1 and Fig. 2, showing the parabolic dish reflector and bistatic receive antenna towards the left. The configuration of the compact range as used for bistatic measurements is summarized in Table I.

TABLE I
COMPACT RANGE MEASUREMENT SPECIFICATIONS

Description	Specifications
Dimensions facility	17.8 m x 9 m x 6.8 m
Receive antenna	Double ridge horn (3dB Beamwidth 40.6° at 12 GHz)
Quiet zone (Monostatic RCS) [13]	1.8 m x 1.8 m x 1.2 m
Polarization	VV
Frequency band measured	2 GHz – 13 GHz
Frequency steps	8.125 MHz
Fixed bistatic angle	30.8°
Target to receiver distance	7.8 m

Although the target is illuminated by a plane wave, the finite separation between the target and the receiver might create a scenario where the physical size of the target is too large and does not adhere to the far-field target to receiver distance requirements, $R \geq \frac{2D^2}{\lambda}$. According to the far-field criteria the maximum target size is limited to approximately 0.764 m at 2 GHz and 0.3 m at 13 GHz. The effect of the finite separation was investigated by comparing near-field simulations in FEKO to the measured data.

Coupling between the receiver and transmitter was eliminated by using time gating during measurements. Calibration was performed with a conducting sphere, diameter 153 mm. The bistatic scattering from the sphere remains constant for bistatic angles around 30.8°, with the frequency response similar to that of monostatic scattering. The raw bistatic measured data and the theoretical bistatic RCS of the sphere was used to calibrate all bistatic measurements.

The bistatic scattering of conducting canonical and complex realistic scale model airframes were measured in the compact range. The simplicity of canonical targets causes certain scattering mechanisms to be emphasized which can be used to accurately compare measured data to simulations. The scattering from complex targets are usually of more importance to radar engineers and were thus also measured in the compact range. The bistatic scattering of a canonical missile and a 1:25 Boeing 707 scale model were measured at a fixed bistatic angle of $\beta = 30.8°$ over a frequency range of 2 GHz to 13 GHz with 1601 points. The dimensions of these targets are listed in Table II.

TABLE II
DIMENSIONS OF THE PEC TARGETS MEASURED IN THE COMPACT RANGE

Target	Dimensions (L x W x H)
Canonical missile	0.95 m x 0.2 m x 0.2 m
Boeing 1:25 scale model	1.9 m x 1.8 m x 0.5 m

Fig. 1. Bistatic measurement setup of the canonical missile.

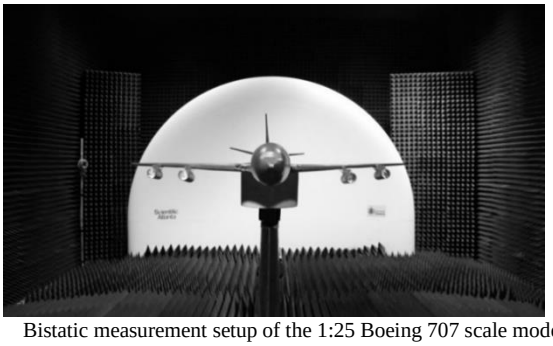

Fig. 2. Bistatic measurement setup of the 1:25 Boeing 707 scale model.

III. SIMULATION SETUP

The CAD model of the canonical missile was created in FEKO. The 1:25 Boeing 707 scale model was laser scanned by the Council for Scientific and Industrial Research (CSIR), South Africa, and imported into FEKO. This is a very accurate representation of the actual model measured in the compact range.

The accuracy of the bistatic RCS measurements performed in the compact range were investigated by comparing the measured data to full-wave simulations. The full-wave simulations were conducted in FEKO using the MFLMM solver. The finite separation between the target and receiver was investigated by comparing near-field simulations in FEKO to the measured data. These near-field simulations approximate the exact measurement setup in the compact

range. This is achieved by placing a near-field probe at the finite distance and bistatic angle of the receiver in the compact range. The near-field simulation setup is illustrated in Fig. 3.

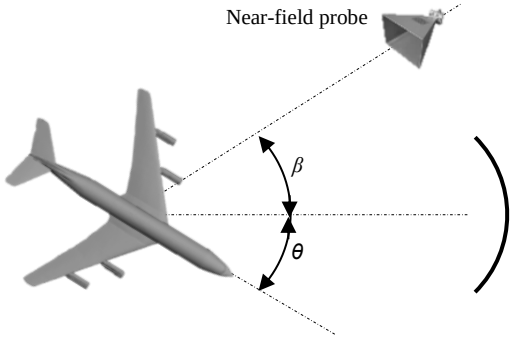

Fig. 3. Near-field bistatic simulation setup for the Boeing scale model. The target is illuminated with a plane wave and the scattering calculated with a near-field probe at the position of the receive antenna at a fixed distance and bistatic angle $\beta = 30.8°$. The target was rotated in azimuth, θ.

IV. Results

At 3.6 GHz the canonical missile has an electrical size of 11λ. The canonical missile did not adhere to the far-field target to receiver distance criteria and the effect of the finite separation between the target and receiver was investigated. The missile required a far-field distance of approximately 22 m at 3.6 GHz. The accuracy of the measured data was determined through comparison with near-field simulations as illustrated in Fig. 4.

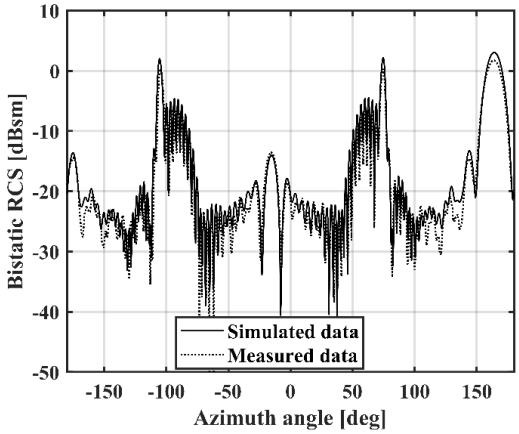

Fig. 4. Measured and simulated bistatic RCS of the canonical missile, VV-pol, 3.6 GHz, $\beta = 30.8°$. At 3.6 GHz the missile had an electrical size of 11λ.

The results are compared in terms of the lobing structure, null-positions and amplitude differences between the measured and simulated data sets. The maximum difference between the measured and simulated data, at the specular scattering caused by the back cone of the missile (at 164°), is 1.3 dB. The maximum difference in the first side lobe is 1.38 dB with a 0° offset. There is a 0.57 dB difference between the measured and simulated data at the peak return caused by the scattering from the front cone of the missile, at -15.5°. There is a maximum difference in the first side lobes of 0.34 dB. A 1.6 dB difference is noted between the measured and simulated data at the specular return, at -105.5° and 74.5°, produced by the cylinder section of the missile. These peaks are caused by the largest scattering feature of the canonical missile viz. the circular cylinder. If the illumination of a target is not sufficient the target will seem electrically smaller and will cause the main lobe to decrease [14]. In this case, the target is sufficiently illuminated by the incident plane wave but the scattering is not in the far-field.

The FSV tool [15], was used for the quantitative comparison between the measured and simulated data for the canonical missile, and is shown in Fig. 5. The FSV method was used to investigate the agreement between the measured and simulated data sets on a more quantitative manner. The FSV mimics the "group mean" approach and divides the data into two parts viz., (i) amplitude data and (ii) feature data. It aims to describe the data by using natural language descriptors. The amplitude difference measure (ADM) output of the FSV comprises of a point-to-point comparison of two input datasets and a probability density function that shows the proportion of the point-to-point analyses. The range of values for these parts can be divided into six categories viz., Excellent, Very Good, Good, Fair, Poor and Very Poor. Almost 100% of the ADM assessment results fall in the first three categories. This is also evident by a visual inspection of the data. The FSV method clearly illustrates that there is very good agreement between the measured and full-wave simulated datasets.

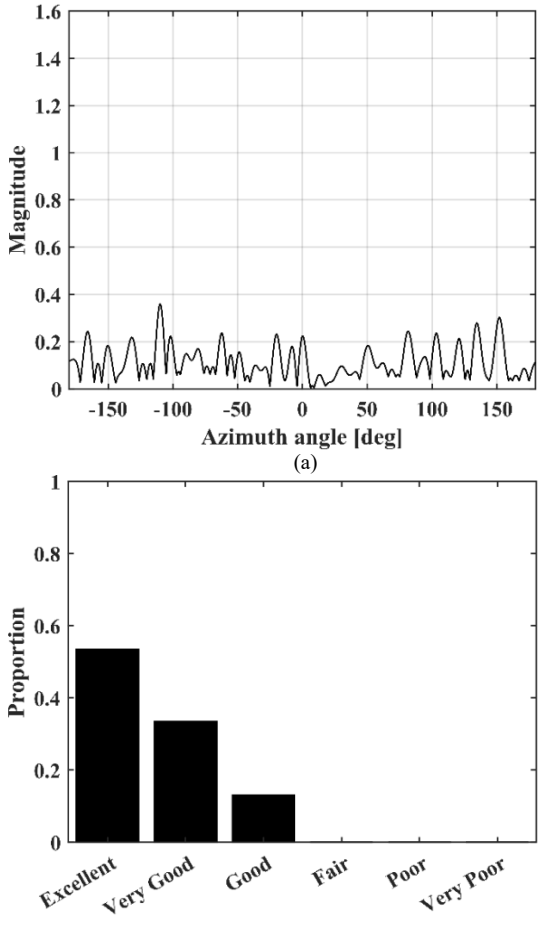

Fig. 5. FSV method applied to measured and simulated data sets of the canonical missile, VV-pol, 3.6 GHz, $\beta = 30.8°$, a) ADM point-to-point results for the missile and b) ADM confidence histogram.

The bistatic scattering of the missile at a higher frequency of 7.505 GHz, is provided in Fig. 6. At this frequency the missile is 24λ long. It seems that the scattering at the higher frequency resulted in a slightly higher correlation between the measured and simulated datasets. At the front of the missile a larger difference of 3 dB is noted between the measured and simulated data. At the specular scattering regions there is a slightly better agreement between the

measured and simulated data sets. A 0.3 dB difference is noted between these two datasets. At the back of the missile a smaller difference of 0.65 dB was noted. The FSV method was also used to evaluate the trend between the datasets as illustrated in Fig. 7. The ADM assessment illustrates that the simulated data correlates well with the measured data as 74% of the trend falls in the "excellent" category. Almost one-hundred per cent, 99.9%, of the ADM results fall in the first three categories.

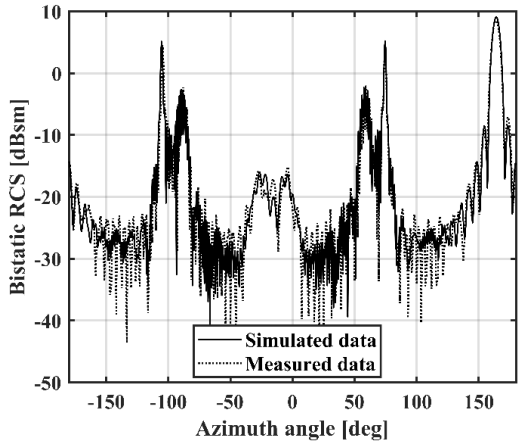

Fig. 6. Measured and simulated bistatic RCS of the canonical Missile, VV-pol, 7.505 GHz, β = 30.8°.

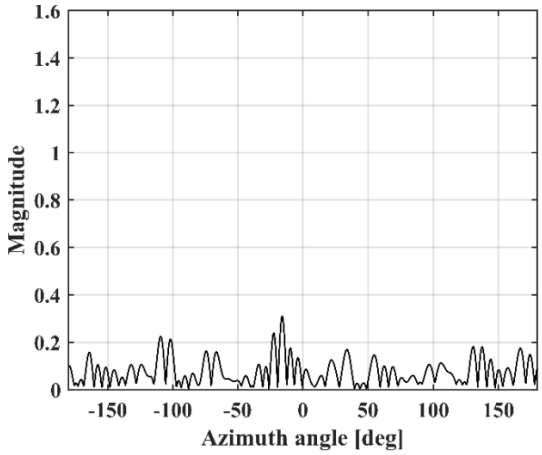

(a)

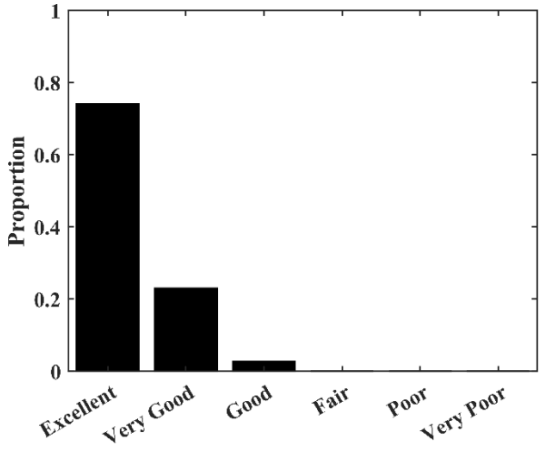

(b)

Fig. 7. FSV method applied to measured and simulated data of the canonical missile, 7.505 GHz, β = 30.8°, a) ADM point-to-point results for the missile and b) ADM confidence histogram.

The bistatic scattering of the complex 1:25 Boeing 707 scale model was also measured in the compact range and simulated in FEKO. At 3.6 GHz a far-field distance of approximately 87 m is required. The measured and simulated results are presented in Fig. 8. The largest scattering feature is observed when the fuselage of the aircraft produces specular scattering toward the receiver, at -105° and 75° azimuth, where differences between the measured and simulated results of 2.6 dB and 0.5 dB are noted, respectively. The large difference between measured and simulated data at -130°, is most probably due to shielding of the scattering from the port side engines by the pedestal. The lobing structure of the measured and simulated data around the peak scattering is in good agreement.

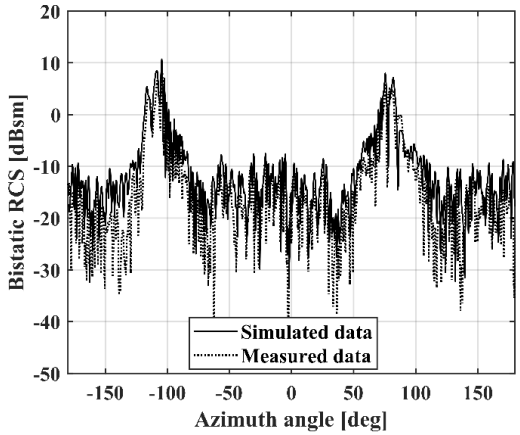

Fig. 8. Measured and simulated bistatic RCS of the 1:25 Boeing 707 scale model, VV-pol, 3.6 GHz, β = 30.8°. At 3.6 GHz the Boeing has an electrical size of 23λ.

The bistatic RCS results for the Boeing scale model at a higher frequency (12 GHz) are shown in Fig. 9. At 12 GHz the required distance between the target and receiver, to comply with the far-field criteria, is 146 m. With a visual inspection it is noted that the overall trend of the datasets are in agreement. Differences are noted at the broad side flashes of the Boeing (around 75° azimuth). At this higher frequency the two wing flashes are more prominent at -55° and 24°. The large difference between measured and simulated results at 100° is most probably due the pedestal obscuring the starboard side engines from the incident plane wave.

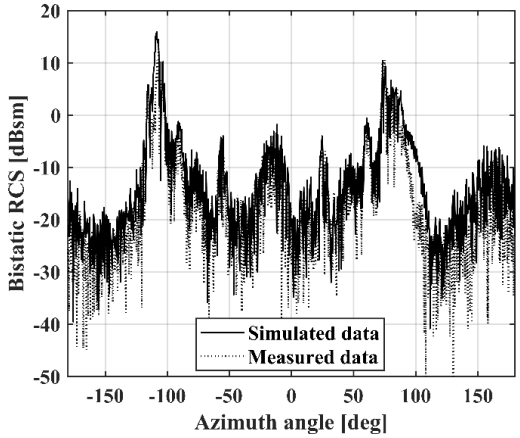

Fig. 9. Measured and simulated bistatic RCS of the 1:25 Boeing 707 scale model, VV-pol, 12 GHz, β = 30.8°.

The FSV method was applied to the measured and simulated data and the ADM results are shown in Fig. 10. The assessment results of the ADM fall with a portion of 42.2% of the trend data, mainly in the

"good" category. Seventy-six per cent of the trend assessment results fall in the first three categories, with 30% in the "fair" category.

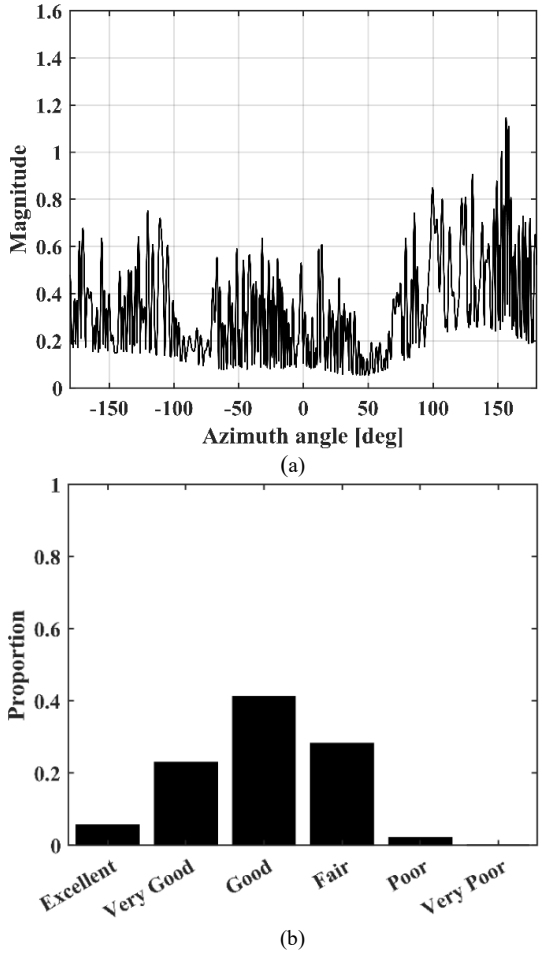

Fig. 10. FSV method applied to measured and simulated data sets of the 1:25 Boeing 707 scale model, VV-pol, 12 GHz, β = 30.8°, a) ADM point-to-point results and b) ADM confidence histogram.

Receiver centric bistatic ISAR images were generated using [16] with the time delay function modified to account for the finite distance between the target and receive antenna. Bistatic ISAR images were generated from -90° to 14°, where scattering is evident from the leading edge of the wing and the engine inlets, and a frequency sweep from 2.5 GHz to 7 GHz, to further investigate the differences between measured and simulated results. The measured and simulated images are provided in Fig. 11 and Fig. 12, respectively. The location and amplitude of the large contributions from the four closed off engine inlets are in good agreement. A maximum difference of 0.7 dB is noted between the measured and simulated scattering from the closed-off engine inlets. The positions and amplitudes of the returns from the nose of the aircraft, the leading edge of the wing and tail are also in good agreement. These two ISAR images further illustrate that good bistatic RCS measurements were performed in the compact range over these angular regions and frequency bands.

Bistatic ISAR images were also generated from -130° to -80°, with dominant scattering from the corner reflector at the tail and the specular reflection from the fuselage. These images were generated over a frequency sweep from 2.5 GHz to 7 GHz. The measured and simulated images are provided in Fig. 13 and Fig. 14, respectively. The location and amplitude of the large contribution from the corner reflector at the tail are in good agreement. A maximum difference of 0.25 dB is noted between the measured and simulated scattering. The position and amplitude of the return from the fuselage of the aircraft and from the sides of the engines are also in good agreement. A larger flash is noted at the left tail of the Boeing in the simulated data compared to the measured data This seems to be a numerical artefact (sidelobe) from the dominant scattering at the tail, introduced by ISAR processing, because it appears "in front" of the target.

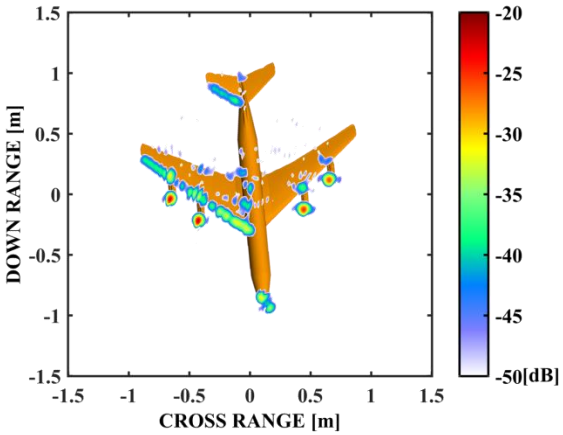

Fig. 11. Bistatic ISAR image: measured data of the 1:25 Boeing 707 scale model, VV-pol, 2.5 GHz to 7 GHz, θ = -90° to 14° (θ = 0° corresponds to the nose-on position of the incident plane wave), β = 30.8°.

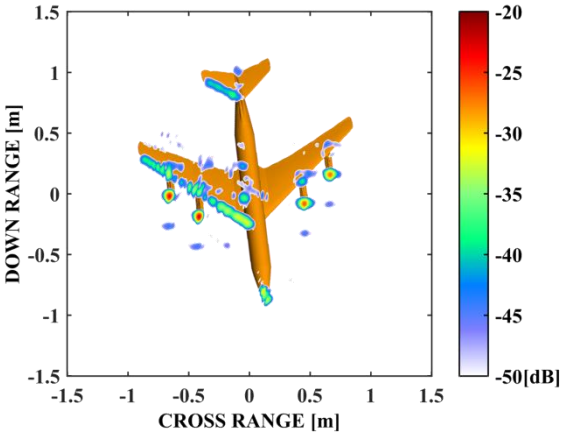

Fig. 12. Bistatic ISAR image: simulated data of the 1:25 Boeing 707 scale model, VV-pol, 2.5 GHz to 7 GHz, θ = -90° to 14° (θ = 0° corresponds to the nose-on position of the incident plane wave), β = 30.8°.

Comparing the measured and simulated RCS results, overall from a visual perspective, the two datasets agree fairly well over the aspect ranges with dominant scattering (larger than -20 dBsm). The half power beamwidth of the receive antenna at 12 GHz is 40.6°, which corresponds to a target size of 5.6 meter. Considering the results in Figures 4 and 6, the beamwidth of the receive antenna at 3.6 GHz is much wider than at 7.505 GHz, yet the specular scattering of the missile is in better agreement at 7.505 GHz compared to 3.6 GHz. A possible cause is the phase variation of the incident wave is slightly larger at the lower frequency. At the lower RCS regions, the results at 3.6 GHz agree better than at 7.505 GHz, this is expected due to generally higher signal-to-noise ratios at the lower frequencies. Because of the complexity of the large Boeing target visible differences between measured and simulated results exist at both frequencies for aspects regions around -130° and 100°. During measurement some parts of the target (e.g. engines) are obscured from the incident wave or receive antenna by the pedestal, while the simulations are performed in free space.

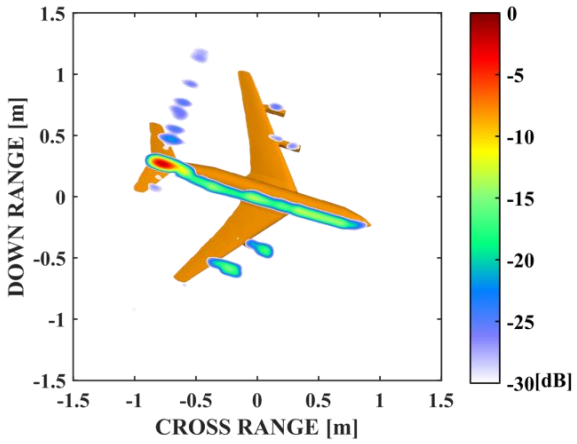

Fig. 13. Bistatic ISAR image: measured data of the 1:25 Boeing 707 scale model, VV-pol, 2.5 GHz to 7 GHz, θ = -130° to -80° (θ = 0° corresponds to the nose-on position of the incident plane wave), β = 30.8°.

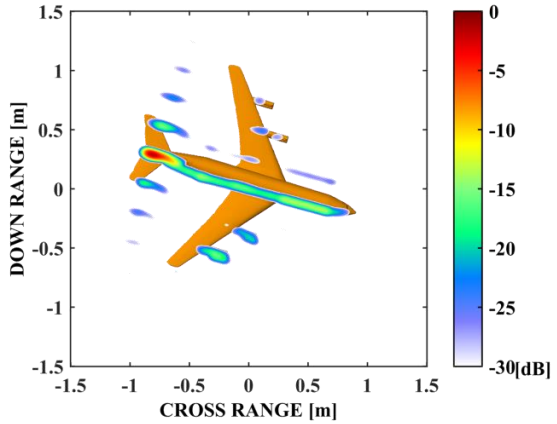

Fig. 14. Bistatic ISAR image: simulated data of the 1:25 Boeing 707 scale model, VV-pol, 2.5 GHz to 7 GHz, θ = -130° to -80° (θ = 0° corresponds to the nose-on position of the incident plane wave), β = 30.8°.

V. Conclusion

A compact range was adapted to perform fixed bistatic RCS measurements. The targets are illuminated by a plane wave created by an offset parabolic dish reflector. The bistatic scattering from the targets are received with a bistatic receiver positioned at a fixed bistatic angle and finite distance from the target. The limitation of this setup is the finite distance between the target and the receive antenna, which is restricted by the physical size of the anechoic chamber. The minimum achievable bistatic angle will be limited by the size of the parabolic reflector as the receive antenna cannot be placed in front of the dish. The accuracy of the measurements performed in the compact range was investigated and the measurement setup was compared to full-wave simulations using MLFMM in FEKO. The measured and simulated bistatic RCS results were analyzed with the FSV method, specifically looking at the ADM results which provides a qualitative point-to-point comparison between the envelopes of the datasets. The majority of the correlation between the measured and simulated data of the FSV assessment for the electrically large targets falls within the first three categories, viz. Excellent, Very Good and Good. From the ISAR images it is also evident that good agreement was achieved between the measured and simulated datasets.

Acknowledgements

The authors are grateful for the support received from Nic Minnaar and Ernst Burger from Altair with the preparations of the CAD models for EM simulation purposes. The support and resources from the Center for High Performance Computing from the Research Institute in Cape Town, South Africa are gratefully acknowledged. This work is based on the research supported by the National Research Foundation (NRF) of South Africa (Grant Number 114941).

References

[1] D. C. Chang, T. Z. Chang, R. C. Liu and I. J. Fu, "Measurement of bistatic radar cross section in sa 5751 compact range," in *Antennas and Propagation Society International Symposium*, Ann Arbor, MI, USA, 1993.

[2] C. W. Pistorius, G. Clerici and W. D. Burnside, "A dual chamber compact range configuration," in *Antennas and Propagation Society International Symposium*, Blacksburg, USA, 1987.

[3] L. Gurel, H. Bagci, J. C. Castelli, A. Cheraly and F. Tardivel, "Validation through comparison: Measruement and calculation of the bistatic radar cross section of a stealth target," *Radio Science*, vol. 38, no. 3, 2003.

[4] F. Daout and F. Schmitt, "Analysis of a bistatic Radar Cross Section measurement capability for the Boris Vian anechoic chamber," in *IEEE Conference on Antenna Measurements & Applications (CAMA)*, France, 2014.

[5] R. A. Marr, U. H. W. Lammers, T. B. Hansen, T. J. Tanigawa and R. V. McGahan, "Bistatic RCS Calculations From Cylindrical Near-Field Measurements - Part II: Experiments," *IEEE Transactions on Antennas and Propagation*, vol. 54, no. 12, pp. 3857 - 3864, 2006.

[6] Altair, "FEKO - Hyperworks, 2018 Release," altairhyperworks.com.

[7] A. Duffy, A. Martin, G. Antonini, A. Orlandi and C. Ritota, "The feature selective validation (FSV) method," in *Proceedings of the IEEE International Symposium on Electromagnetic Compatibility*, Aug. 2005.

[8] C. J. Bradley, P. J. Collins, J. Fortuny-Guasch, M. L. Hastriter, G. Nesti, A. J. Terzuoli and K. S. Wilson, "An investigation of bistatic calibration objects," *IEEE Transactions on Geoscience and Remote Sensing*, vol. 43, no. 10, pp. 2177-218, 2005.

[9] C. J. Bradley, "The calibration of bistatic radar cross section measurements," Air Force Institute of Technology Thesis, USA, 2001.

[10] D. C. Chang, C. H. Liao and C. C. Wu, "Compact antenna test range without reflector edge treatment and RF anechoic chamber," *IEEE Antennas and Propagation Magazine*, vol. 46, no. 4, pp. 27 - 37, 2004.

[11] M. Pienaar, J. W. Odendaal, J. Joubert, C. Pienaar and J. C. Smit, "Bistatic RCS measurements in a compact range," in *ICEAA IEEE APWC*, Verona, Italy, 2017.

[12] M. Pienaar, J. W. Odendaal, J. Joubert, J. C. Smit and J. E. Cilliers, "Active calibration target for bistatic radar cross-section measurements," *Radio Science*, vol. 51, no. 5, pp. 515-523, 2016.

[13] S. Atlanta, Instruction Manual Model 5754 Compact Antenna Range, June 1987.

[14] R. Gente, C. Jansen, R. Geise, O. Peters, M. Gente, N. Krumbholz, C. Moller, S. Busch and M. Koch, "Scaled Bistatic Radar Cross Section Measurements of Aircraft With a Fiber-Coupled THz Time-Domain Spectrometer," *IEEE Transactions on Terahertz Science and Technology*, vol. 2, no. 4, pp. 424-431, 2012.

[15] University of L'Aquila, Italy, "UAq FSV Tool," [Online]. Available: http://orlandi.ing.univaq.it/pub/FSV_Tool_20/.

[16] R. Burkholder, I. Gupta and J. Johnson, "Comparison of monostatic and bistatic radar images," *IEEE Antennas and Propagation Magazine*, vol. 45, no. 3, pp. 41-50, 2003.